Variability of Active Galactic Nuclei from Differential Photometry

A Senior Thesis Presented to
the Physics Department of
California Polytechnic State University
San Luis Obispo

In Partial Fulfillment
of the Requirements for
the Physics Degree
Bachelors of Science

By
Nicholas S. Yee

Advised By
Vardha N. Bennert

September 2020

1   Abstract

The Seoul AGN Monitoring Project, or SAMP for short, is an international project (PI Jonghak Woo from Korea) with the goal of measuring the masses of black holes residing in the center of massive active galactic nuclei (AGNs). AGNs are some of the brightest objects in the universe. Their light is attributed to the accretion of material onto the black hole. However, these objects are too distant to spatially resolve the gravitational sphere of influence of the black hole directly. Instead, we use a technique called reverberation mapping which observes the variability of the AGN power-law continuum emission and the time-delayed response of gas clouds ionized by the AGN that orbit the black hole inside the so-called broad-line region (BLR). Knowing the speed of light, the observed delay can be translated into the size of the broad-line region. Including the width of the broad emission lines, which is a tracer of the velocity of the BLR clouds, we can estimate the mass of the black hole. Photometry of the AGN optical continuum emission gathered from the 1m Nickel telescope at Lick Observatory is combined with spectroscopy of the BLR of the same AGNs obtained with the 3m Shane telescope at Lick Observatory. Students at Cal Poly have been in charge of the 1m Nickel telescope observations from January 2017 to September 2019, by operating the 1m telescope remotely from Cal Poly. In this thesis, I will cover the process of obtaining these optical images and analyze the continuum variability of the AGNs. In total, I present light curves for 18 AGNs, all of which show at least some degree of variability, promising successful black hole mass measurements when combined with spectroscopy results.

2   Introduction

2.1   AGN Overview

Active Galactic Nuclei (AGNs) are objects that lie within the center of galaxies and emit energies much greater than their host galaxy. The two largest sub-classes of AGN are Seyferts and quasars. Seyferts are known to have nuclear sources on the order of $1 \times 10^{11}\,\mathrm{L_\odot}$, while quasars have energy at $1 \times 10^{13}\,\mathrm{L_\odot}$ (with $\mathrm{L_\odot}$ being the solar luminosity of the Sun) or greater. AGNs have similar characteristics such as they are star-like objects with a time-variable, continuum flux, a large ultra-violet flux, and large red-shift. This information summarized in this chapter is taken from An Introduction to Active Galatic Nuclei by Bradley Peterson, published February 13, 1997.
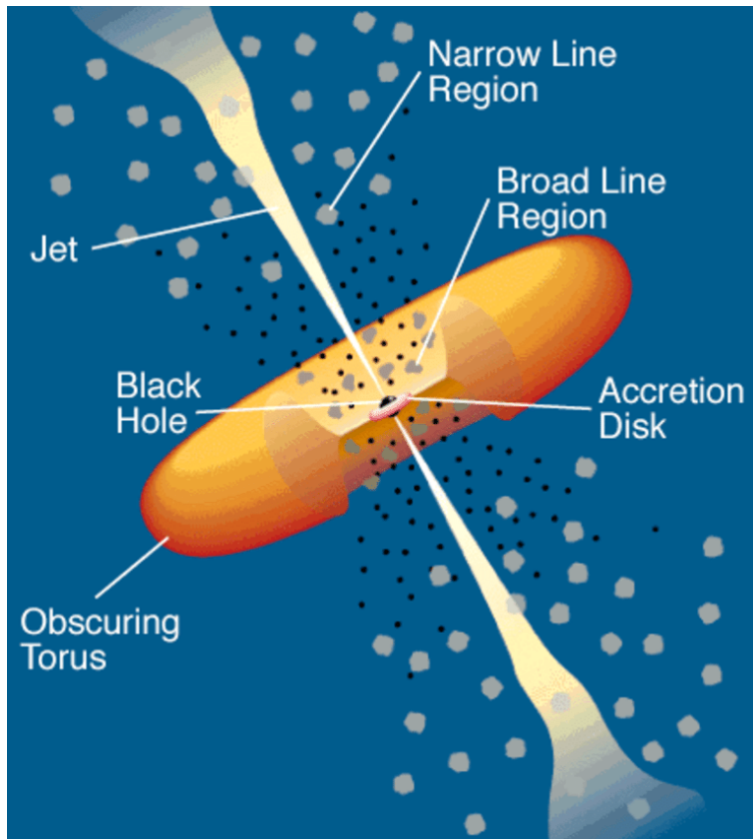
Figure 1: The Unified Model of an AGN with labeled parts
(Urry and Padovani, 1995)

2.2 AGN Components

2.2.1 Accretion Disk

The accretion disk is a region in which matter gathers around the black hole. In the accretion disk, gravitational potential energy is converted into light via friction. The disk heats up and emits locally like a black body. The sum of the localized blackbody spectra is a power-law continuum with emission in the UV-optical. The disk is responsible for much of the energetic properties observed from AGN. The energy is due to the frictional forces of the matter within the disk itself. Accretion disk are stable due to the outward radiation pressure force counteracted by the inward gravitational force. The radii of most accretion disks are between 1 pc < r < 100 pc and the black hole at the center has a mass of ranging from $M^{9\pm1}M_{sun}$.

2.2.2 The Broad Line Region

The broad line region (BLR) is important because of its relationship with the central source. The black hole's gravitational pull causes the BLRs bulk motion. The region has orbital velocities ranging from 500 km/s-5000 km/s. Broad lines in the BLR are Doppler-broadened and are calculated by either the intensity of the full width half max (FWHM) or the full width zero intensity (FWZI). However, the FWZI is more uncertain because other lines can combine with this one. The BLR has some unique features. For example, the light emitted by the accretion disk ionizes the gas in the BLR region, which explains why the emission lines have fluxes that correlate with the continuum flux. When electrons recombine with the ionized hydrogen atoms (protons), light is emitted in the form of the Balmer emission lines. It is also thought that a majority of recombination lines come from optically thick clouds in the ionizing continuum. The BLR is dense because there are no forbidden lines that are broad, which means it is more likely that an excited electron to become de-excited due to collision rather than from transitioning of orbital states and emission of light. Forbidden lines are emission lines that are typically prevented from a quantum-mechanical selection rule and can thus be easily collisionally suppressed, meaning that the electron is de-excited through collisions in high density environments rather than by emitting a photon. BLR models mainly depend on the chemical composition, particle density of the cloud, and the ionizing continuum shape.

2.2.3 The Narrow Line Region

The narrow line region (NLR) is the region of the AGN that lies just outside the BLR and is about 100 pc-1000 pc. Unlike the BLR, the NLR has gases with slower orbital velocities ranging from 200 km s^{-1} to 900 km s^{-1}. Within the NLR, forbidden transitions are not collisionally suppressed, which means electron densities are low. When electron densities are low, the radiative process occurs so fast that all collisional excitations are immediately followed by radiative de-excitation. On the other hand, de-excitation happens collisionally

rather than radiatively in high electron densities (for example in the BLR). Temperatures range from 10,000 K to 25,000 K which are measured from the ratio of certain forbidden line pairs. However, there is a dusty torus that lies partly in the NLR because the NLR lies outside the dust sublimation radius of the AGN. Even with this layer of dust, the radius and mass of the NLR can be measured through the luminosity of specific strong lines. In addition, the partially resolvable region is classified as clumpy in high-resolution spectra. However, short-term narrow-line variability is difficult to measure since the NLR is so large (a minimum of 300 light-years wide). Another characteristic of the NLR is that narrow-line emission profiles are often blueward asymmetric and are non-Gaussian with bases that are wider than a normal Gaussian because the outflows of gas head toward Earth (blueshifted). On the other side (the side facing away from Earth), the outflows of gas which would appear redshifted is blocked by dust and so is not seen in the spectra. The NLR widths help describe the gravitational field of stars within the AGN, while the BLR line widths describe the gravitational potential of the black hole. Note that the NLR can merge with the BLR if the density and velocity dispersion increase further in towards the black hole. The NLR is classified as axisymmetric, rather than spherically symmetric, which means the NLR axis has the same radio axis as AGNs where radio emissions occur. Within the NLR there are wedge-shaped structures known as "Ionization Cones" which occur because the flux ratio is larger outside the cone than within. This means the inside of the cone is ionized by the AGN while the outside is either not ionized or ionized by stars. The ionization cones can be classified as single-sided or bi-conical structures.

2.2.4   The Dusty Torus

The dusty torus is the region between the broad line region and the narrow line region. Even though it has been historically called "torus," this dusty region is likely not going to have a doughnut-shape. Today it is more common to refer to it as a toroidal structure, but the dust is likely to be distributed clumpy clouds. It is a region of dust formed outside the so-called dust-sublimation radius, where the temperatures are too hot for dust to exist. Although the torus is small, depending on our viewing angle, can block some of our view of the AGN. The dusty torus is the key ingredient in the so-called Unified Model of AGNs discussed in the next section.

2.3   The Unified Model of AGNs

Two types of AGN are Seyfert-1 galaxies and Seyfert-2 galaxies. One main difference between the two is in the emission spectra. In Figure 2, the broad lines and the power-law continuum of the AGN are visible in Seyfert-1s. However in Seyfert-2s, only the narrow lines are visible and the power-law continuum is not visible but the absorption lines from the underlying stars of the host galaxy are visible. Yet, these differences are thought to be attributed to our viewing angle of the Seyfert galaxies. The dusty torus is the key ingredient in the Unified
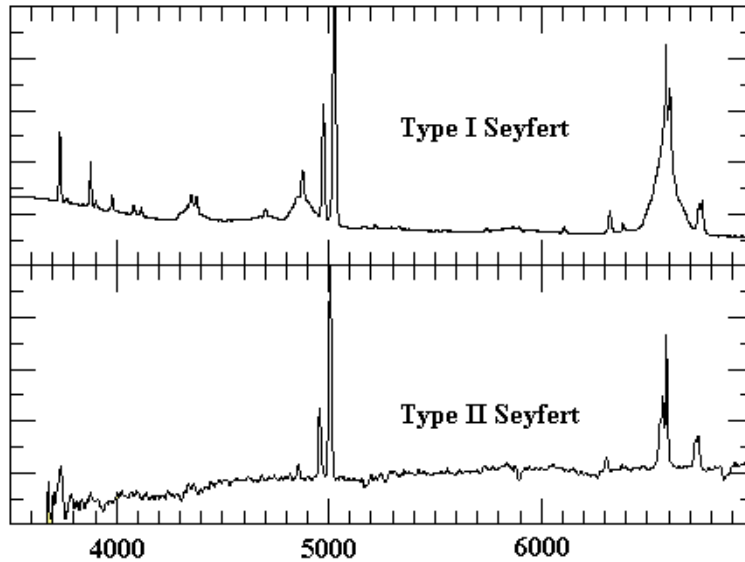
Figure 2: Seyfert-1 and Seyfert-2 spectra. For Type I Seyfert galaxies (upper panel), the emission lines of He II, Hbeta, and Halpha are broad (from left to right). For Type II Seyfert galaxies (lower panel), all emission lines are narrow. (Keel, 2002)

Model of AGNs. If we see the central engine of a Seyfert galaxy "face on," both the broad emission lines from the BLR and the continuum from the accretion disk (power-law continuum) are visible. If, however, we see the central engine of a Seyfert galaxy "edge on," then the dusty torus blocks our view. Thus, many astronomers believe that our perspective is the only factor changing. Evidence of this model arose from observing broad lines in polarized light from Seyfert-2 galaxies due to electrons scattering BLR emission in our perspective.

2.4   Reverberation Mapping

Through a technique called reverberation mapping, we can estimate the masses of black holes at the center of AGNs by collecting the flux of the central source from photometry, the flux of the BLR from spectroscopy, and the velocity of the gas in the BLR using Doppler broadening from spectra in the BLR. We can also calculate the radius of the BLR from comparing the delay between the continuum changes from the accretion disk and the emission lines change in the BLR and the light travel time between the central source and the BLR. The larger the mass of the black hole, the larger the time lag because larger mass means larger luminosities, which can ionize the BLR to a larger radius. The variation in the BLR emission lines is a response to variations in the continuum of the AGN emitted from the accretion disk around the black hole, since that

continuum is the source of ionization of the BLR. From this data we can make light-curves which show how flux changes over time. The number of days between two peaks in flux can be converted to a distance in light days, which is the distance light traveling at the speed of light would travel in those days to give us the radius of the BLR. Using this relation, we can estimate the mass of the black hole:

$$M_{BH} \propto \frac{R_{BLR} \times v_{BLR}^2}{G} \tag{1}$$

3 Seoul National University AGN Monitoring Project (SAMP)

The goal of the Seoul National University AGN Monitoring Project, or SAMP for short, is to measure the masses of black holes within massive AGNs for 35 objects with redshift ranges of z=0.127 to z=0.343 and a masses ranging from 2.10×10^3 M$_{sun}$ to 8.87×10^3 M$_{sun}$. The effort is lead by a group at the Seoul National University in Korea (PI Dr. Jonghak Woo). It also involves people at the University of California Los Angeles (Dr. Tommaso Treu and Dr. Matthew Malkan) and at the University of California Irvine (Dr. Aaron Barth and Dr. Vivian U). To do this, we use the 1m and 3m telescopes at Lick Observatory to observe the light lag times between the accretion disk and the broad line region of the AGN. The project started January 27, 2017 with an observing night occurring about every 10 days. I joined the project November 16, 2018 but did not start officially operating the 1m telescope until I went through the training process that every astronomer needed April 3, 2019. The last observing night officially ended September 5, 2019. In total we had 97 observing nights for the duration of the project. However, there are 57 nights where we were able to successfully gather data. Chance Spencer is a Cal Poly student who joined the project earlier than me and did his senior thesis on all of the nights from 2017-2018. He reduced all those data, but only performed photometry on two objects. In this senior thesis, I reduce data from all the successful nights in 2019 and combine them with the previously reduced data. I then perform photometry on a total of 18 objects.

4   Observations

We arrive an hour or two before sunset to setup the telescope to its proper settings. Once the telescope is good to go, we take about 20 biases and make sure that the bias count is about 1000 (+/- 100 counts). A bias is a zero second exposure with the shutter closed and no photons. Biases only read out count levels and needs to be subtracted out. Right after sunset occurs, is the perfect time to take V and B-filter sky flats because at this time the sky flat counts occur between the optimal range of 20,000 to 50,000 counts. A flat is a flat background that tests the sensitivity of individual pixels, and we want to take out the variability from pixel to pixel by dividing these out from all the other images in this filter. We try to obtain about 6-8 flats in each filter, but if we miss this opportunity due to various issues, we have another chance to take these flats at sunrise. Once the sun sets, we move onto pointing, in which we center the telescope by moving the telescope to bright stars that can easily be seen. After the telescope is correctly pointed, we begin the focusing process. We offset the image of the same star and change the focus slightly. A pop-up window tells us which of the images has the smallest full-width half-max, or FWHM, which translates to the best focused star. We then take exposures of standard stars or star fields of known magnitude. This completes the set up portion of the night. We can now move onto to taking exposures of the objects we want for the night. A list of all the objects observed can be found in Table 1. To find the desired object, we move to it by feeding the coordinates to the graphical user interface and set the exposure time to the desired time. Once the exposure has finished, we check that the image matches the same image in our star charts and if it does, we continue onto the next object. We then repeat the same process for the next object. A standard night will have about 15 objects. Once all of the objects have been recorded we close the telescope and end for the night.

SAMP AGN Objects with Coordinates				
Object Label	RA	Dec	z	B Magnitude
A01	1:01:31	42:29:36.0	0.190	16.7
A03	1:40:35	23:44:51.0	0.320	16.9
A04	2:27:40	44:10:00.0	0.175	18.4
A11	8:01:12	51:28:12.3	0.321	18.6
B01	8:03:09	53:00:04.8	0.287	18.5
B02	8:13:18	43:56:20.6	0.254	17.8
B04	8:48:53	28:24:11.8	0.198	18.3
B06	9:36:09	65:10:54.9	0.192	17.7
A14	9:39:40	37:57:05.8	0.231	18.0
A15	9:50:36	39:29:24.0	0.206	17.1
A18	10:59:36	66:57:58.0	0.340	17.7
B09	11:17:06	44:13:33.3	0.144	16.4
A23	11:20:07	42:35:51.4	0.226	17.8
A26	12:03:48	45:59:51.1	0.343	17.4
A29	12:17:52	33:34:47.3	0.178	17.5
B18	13:23:50	65:41:48.2	0.168	15.9
A32	13:56:33	21:03:52.4	0.300	17.6
A36	14:15:36	48:35:43.6	0.275	17.8
B24	14:29:43	47:47:26.2	0.220	17
B26	14:42:07	35:26:23.0	0.079	15
B27	14:53:34.8	34:31:27.8	0.209	17.9
A38	14:56:09	38:00:38.6	0.283	17.3
A40	15:26:24	27:54:52.1	0.231	17.1
B31	15:35:39	56:44:06.5	0.207	17.8
A41	15:40:04	35:50:50.1	0.164	16.7
B32	15:42:35	57:41:41.9	0.245	18.4
A42	15:47:44	20:51:16.8	0.264	16.3
B35	16:14:13	26:04:16.3	0.131	16.4
A43	16:19:11	50:11:09.2	0.234	17.9
A47	19:35:21	53:14:12.1	0.248	16.1

Table 1: A table of each observed objects' RA, Dec, z, and B magnitude.

5   Data Reduction

In 2019 there were 15 successful nights (marked by the Table 2) in which useable data was collected. To successfully reduce this data, I upload each night's data into the Cal Poly Dirac cluster. Each night's data is uploaded separately into their own respective folders. Within each folder is the data from the observing night and 7 text files with all the useable data that I check before uploading. Using the application, PYRAF, on the Dirac cluster, I average all the useable biases into a masterbias text file. To do this, I specifically use the "epar zero-combine" functions of PYRAF to create the masterbias. Then, I subtract the newly created masterbias from all of the useable images of the night using the "epar ccdproc" function of PYRAF. Next, I do a similar process for the flats. I average out the usable flats for a given filter and create a masterflat in the B and V filters by using the "epar flatcombine" function in PYRAF. Then I divide all object images in a given filter by the corresponding masterflat in that filter. I check that processes were done correctly by checking the images visually in the DS9 application and check that the counts were subtracted correctly (which would be a subtraction of about 1000 counts). This would signify the masterbias subtraction was done successfully. To check that the masterflats were divided out of each image, I check that the overall image is smooth and any flat structures that were in the image previously are now gone. The image above shows the raw image and a reduced image. Notice how the reduced image looks a lot smoother and there are less divots. To learn more about the data reduction process, Chance Spencer's Cal Poly Senior Thesis goes into much greater detail.
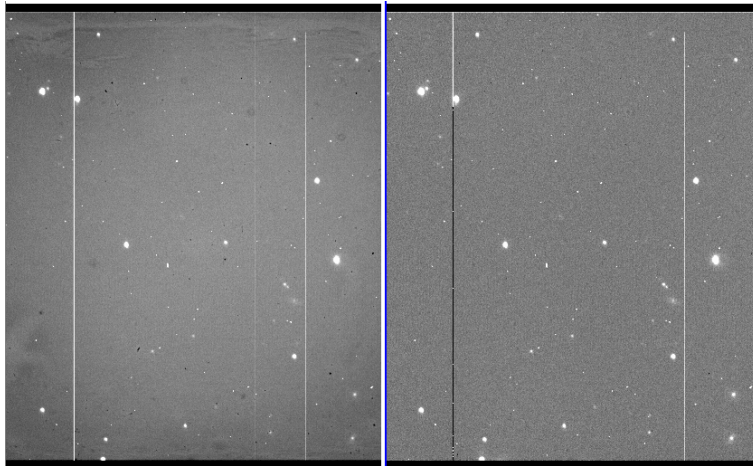
Figure 3: A sample image before and after data reduction

List of 2019 Cal Poly SAMP Team Observation Nights with 1m Nickel			
Date	Data Obtained	Julian Date	Observers
01/13/19	No	2458496	Gibson, Hood, Spencer, **Yee**
01/26/19	Yes	2458509	Gibson, Hood, Salinas
03/01/19	No	2458543	Glad, Gibson, Hood
03/13/19	Yes	2458555	Asaravala, Gibson, Hood, Salinas, **Yee**
03/27/19	No	2458569	Hood, Mendoza
04/05/19	No	2458578	Asaravala, Hood, **Yee**
04/11/19	No	2458584	Glad, Gibson
04/24/19	Yes	2458597	Glad, Hood, Snyder
05/06/19	Yes	2458609	Hood, Salinas
05/13/19	Yes	2458616	Asaravala, **Yee**
05/27/19	Yes	2458630	Gibson, **Yee**
06/04/19	Yes	2458638	Salinas, Snyder
06/11/19	Yes	2458645	Gibson, Hood, Spencer
06/24/19	Yes	2458658	Snyder, **Yee**
07/01/19	Yes	2458665	Snyder, **Yee**
07/08/19	Yes	2458672	Spencer, **Yee**
07/24/19	Yes	2458688	Snyder, **Yee**
07/30/19	Yes	2458694	Snyder, **Yee**
08/03/19	Yes	2458698	Snyder, **Yee**
08/07/19	Yes	2458702	Snyder, Spencer
08/22/19	No	2458717	Spencer, **Yee**
08/30/19	Yes	2458725	Snyder, **Yee**
09/05/19	Yes	2458731	Snyder

Table 2: A table of observing nights from our project during 2019 listed with the date of the night the observations started on, whether data was successfully collected for that night, the reasons we were not able to observe if that was the case, and who the observers were for that given night. For the observing nights in 2017 and 2018, a similar table can be found in Chance Spencer's senior thesis.

6   Data Analysis

After the data is reduced, I collect all of the images of the same object from the different nights into a new directory. If the object is at exactly the same location, then I combine and average the images if they are from the same night using the command "imcombine". Using the correct parameters that are illustrated in Chance's senior thesis, I use the command "daofind" to create .coo files. These files contain coordinates of stars that the program found in a given image. However, I only want the coordinates of the comparison stars and AGN. To do this, I locate the AGN and 4 comparison stars I want to use by displaying each image in DS9 and clicking on the star or AGN. This creates a green circle around the star or AGN. I type "imexam" and the letter "s" which creates a Gaussian curve of the flux of the star or AGN to makes sure the program detects the object. Then I type the letter "a" to find the coordinates of each object I want and record it in an excel sheet. Next, I need to delete all the objects in the .coo file and manually input the coordinates of the objects I want, which are recorded in the excel sheet I just created. Now the object is ready for photometry. Using the command "phot", creates .mag files which list the flux of each desired object. I record the magnitudes of each comparison
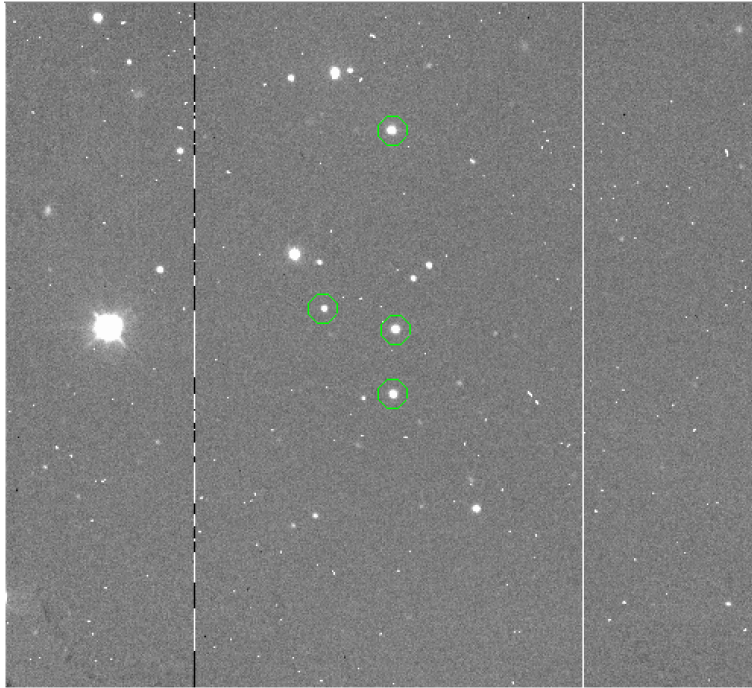
Figure 4: A picture of the comparison stars I chose to use for the differential photometry.

star in a new excel sheet. Then I average out the magnitudes of the comparison stars and subtract this value from the magnitudes of the AGN. Also in this new excel sheet, I convert the time and date of which the objects were taken to Julian date using an online converter. I am now ready to create the light curve by plotting the time (in Julian date) against the difference in flux between the AGN and the averaged out comparison stars. The following pages contain the finished light curves for objects A38 and the rest of the light curves can be found in the appendix.

7   Results and Discussion

Below is the light curve for A38. Chance Spencer included in his senior thesis light curves of A38 and A43 but did not include the 2019 observations because he graduated before then. The parts of the graph that do overlap may differ due to the difference in aperture size (I used a size of 8 based on the curve of growth while Chance used 7.) In addition, I used an annulus of 15 and a dannulus of 5 in the "fitskypars" GUI, while Chance used an annulus of 20 and a dannulus of 15, which could explain the discrepancies in our data. From the data, we can see that the A38 light curve has a magnitude difference of at least 0.747 mag. There is one outlier with relatively large error bars. I included a second graph of A38 without the outlier to better see the overall variability. In total, I created light curves for 18 objects. They are shown in the appendix, including images of the comparison stars used. Comments on individual objects can be found in Table 3. In this table, I broadly classify the light curves into three categories: if less than 0.1 mag difference in between widest range: not variable, if between 0.1-0.4 mag difference in between the widest range: variable, if greater than 0.4 mag difference in between the widest range: highly variable. All objects have been classified as variable. 7 objects have been classified as highly variable. All objects show at least some degree of variability, promising successful measurements of the black hole masses, once the photometry is combined with the spectroscopy of the 3m telescope. This thesis contains 18 light curves out of 30 objects. I focused on those objects that were observed over many nights (meaning they have many data points.) Of the remaining objects still to be analyzed, 9 objects with 10-15 data points and 3 objects with less than 10 data points are still left.

Note of caution: a possible issue is that the AGN lives in a host galaxy, so depending on the aperture and seeing, there could be more or less flux of the host galaxy being artificially added to the AGN flux, causing a variability that is not due to the AGN. There is nothing we can do about this problem, using simple aperture photometry. The only way around would be to do a sophisticated fitting and subtraction of the host galaxy, but this is beyond the purpose of this thesis. Moreover, the AGNs in these quasars are very bright and the host galaxy typically faint, so we do not expect this to be a dominant source of error.
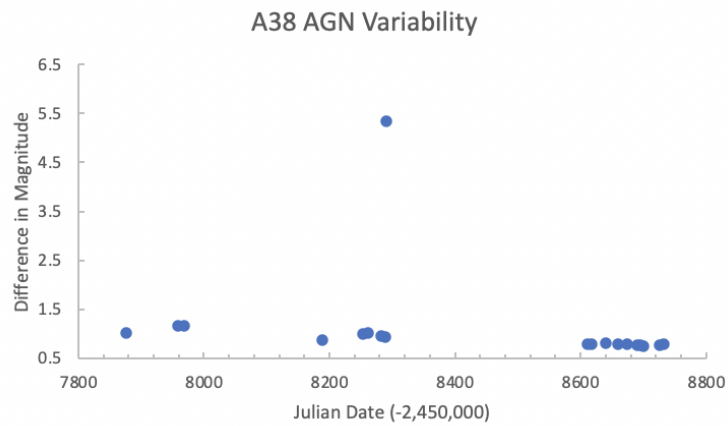
Figure 5: The light curve for A38 shows the difference in magnitude between the AGN and the average of a 4 comparison stars, as a function of time in Julian Date (in days).
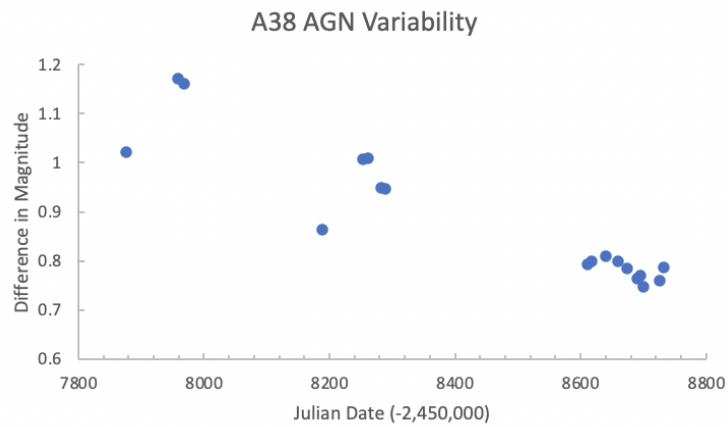
Figure 6: This light curve is the same as the light curve in Figure 5 but without the outlier.

Object Name	Variability	Comments
A01	Variable	$-----$
A03	Highly Variable	$-----$
A04	Variable	Several images were blurry and unusable
A11	Highly Variable	$-----$
A18	Variable	$-----$
A36	Variable	Huge error bar on one of the points
A38	Highly Variable	$-----$
A40	Highly Variable	$-----$
A41	Variable	One outlier
A42	Highly Variable	$-----$
A43	Variable	Huge error bar on one of the points
A47	Variable	$-----$
B06	Highly Variable	$-----$
B18	Variable	$-----$
B24	Highly Variable	One outlier
B26	Variable	Huge error bars on one of the points
B31	Variable	$-----$
B35	High Variability	$-----$

Table 3: A table of the light curves finished, classification of variability of those light curves, and comments on the light curves.

8   Summary

In this thesis, I present data obtained at the 1m Nickel telescope of Lick observatory between January 2017 and September 2019. The observations were carried out by Cal Poly undergraduate students, including myself. This was part of an international collaboration (PI Jonghak Woo, Korea), called the Seoul AGN Monitoring Project (SAMP), with the goal to measure the mass of the black hole in the center of these active galaxies. Here, I present data reduction and differential photometry for 18 objects in the sample. The light curves created show that all AGNs are variable, many of them highly variable. When combined with results from the spectroscopy carried out at the 3m Shane telescope of Lick observatory, the masses of the black holes can be determined, but this is beyond the scope of this thesis.

9   Acknowledgements

10   Appendix

A   Re-configuring Images

When displaying an image in DS9 and locating comparison stars, the way that
the Nickel fits files are saved does not preserve the astronomical default for
imaging that North is up and East is to the left. To rotate the image in the
right orientation (such that North is up and East is to the left), I click the zoom
header, click "invert x", and "click 180 degrees." In the figures below show when
the image is first displayed in the wrong orientation and after the image has been
correctly orientated. This is important for comparison with the finding charts,
which are by default oriented such that North is up and East is to the left.
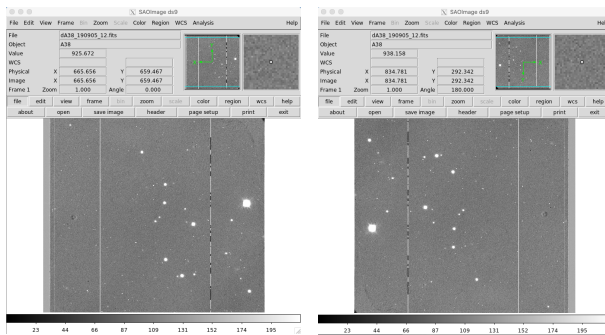
Figure 7: This is how the
image first appears when
loaded onto DS9, notice
how the comparison stars
are inverted in the x and
y directions

Figure 8: This is the re-
sult of the correctly orien-
tating the image. Notice
how this matches the im-
age of locating the com-
parison stars and AGN.
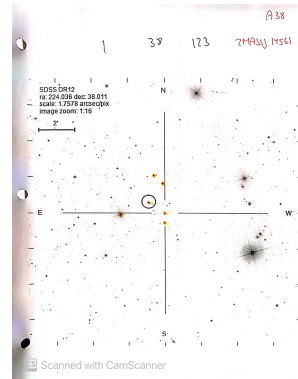
Figure 9:   This is the
finding chart used to ver-
ify the image we have
matches the the finding
chart.   Notice how the
field of view is larger here
than in the images.

16

B   Creating a Growth Curve

When setting up the right parameters for the Data Analysis section, a growth curve helps determine what aperture number should be used for photometry. I first copy 3 of the images into a subdirectory (a bad seeing, intermediate seeing, and best seeing image) where I change the coordinate files to measure the magnitude of one comparison star with no neighboring stars and the smallest FWHM. I change the parameters of the command "photpars" to list the apertures from 2-15. Next, I run the photometry to get the magnitude for each aperture number. I record the magnitudes at the different aperture numbers and plot the two against each other in an excel spreadsheet. From the images, the best aperture is the point of the graph where the peak stops increasing exponentially and starts to flatten out. This point was around an aperture number of 8.
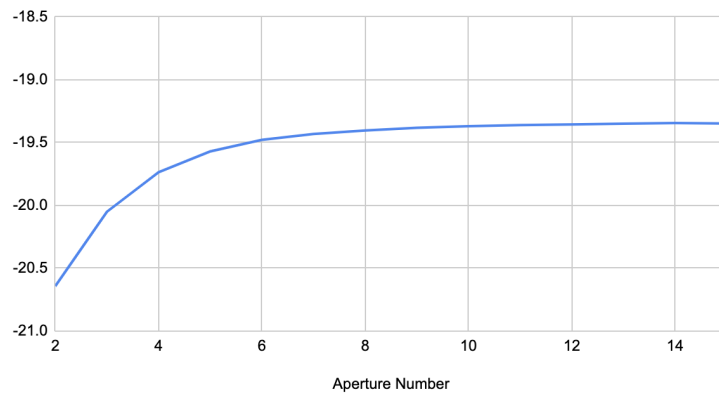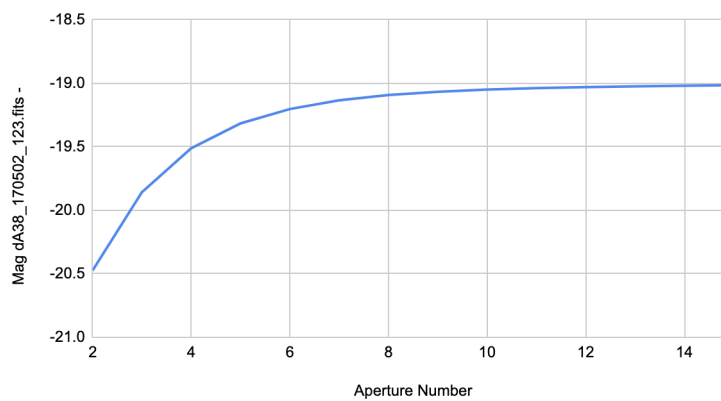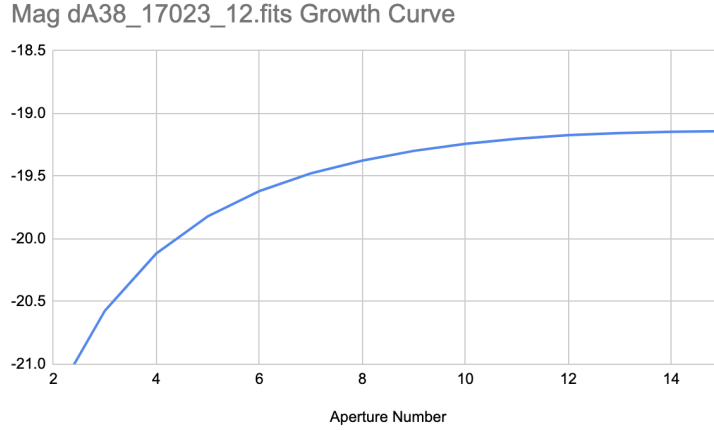
Figure 10: The best aperture varies from image to image but the general best aperture out of the 3 images is an aperture number 8. Note: the y-axis should be positively-reversed, so to bypass this I used a negative sign (so the negative sign can be ignored).

C   Calculating Error

The command "txdump *.mag.1 merr," lists the error for each comparison star and AGN I manually input into the .coo files. Next I use the formula below to find the total error for the difference in magnitude between the AGN and the comparison stars. Once I have created the light curve, the added error bars in excel are generic values and not the specified values I just calculated. Under the "Chart Design" tab, "Add Chart Element," there is an "Error Bars" tab. Within the "Error Bars" tab, I click the "More Error Bars Options" which leads to the "Custom" option on the right side of Excel. From there I highlight the column of the calculated error, which gives the desired error values I want.

$$\sigma_{total} = \sqrt{\sigma_{Star1}^2 + \sigma_{Star2}^2 + \sigma_{Star3}^2 + \sigma_{AGN}^2} \tag{2}$$

D Objects with their Chosen Comparison Stars and Light Curves
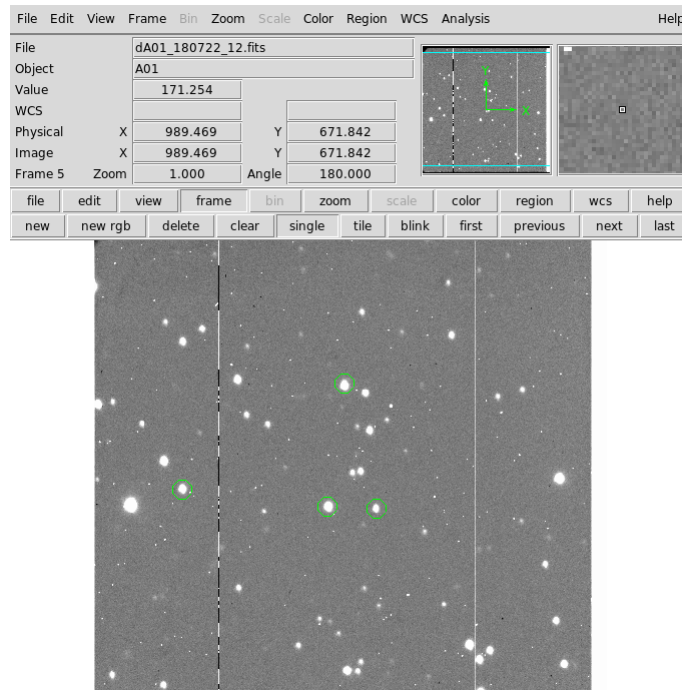
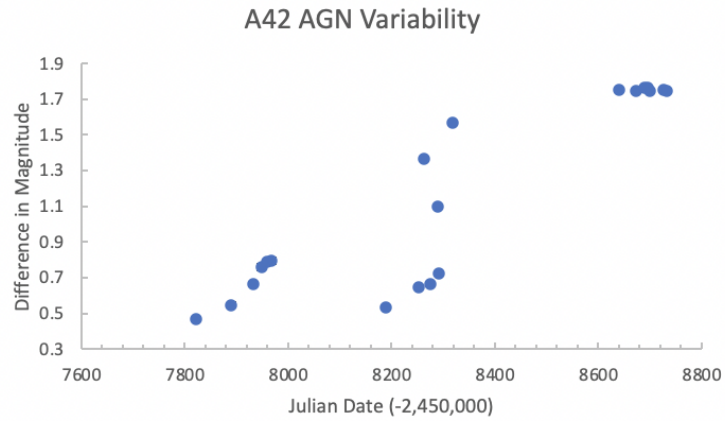
Figure 11: Comparison Stars used for object A01.
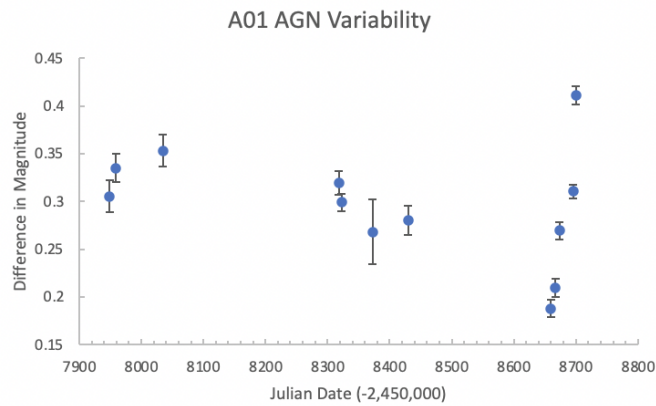
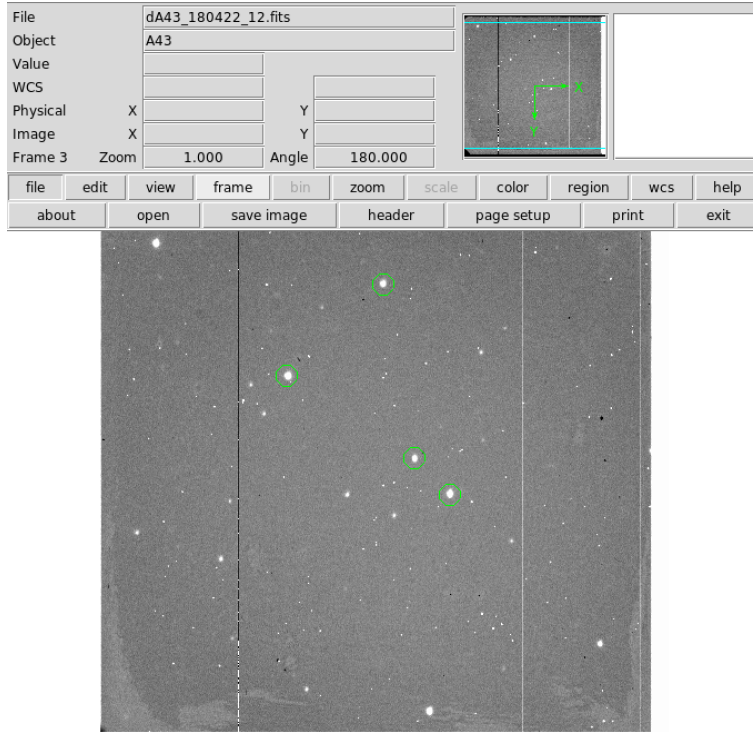Figure 12: The same as in Figure 5 for object A01.
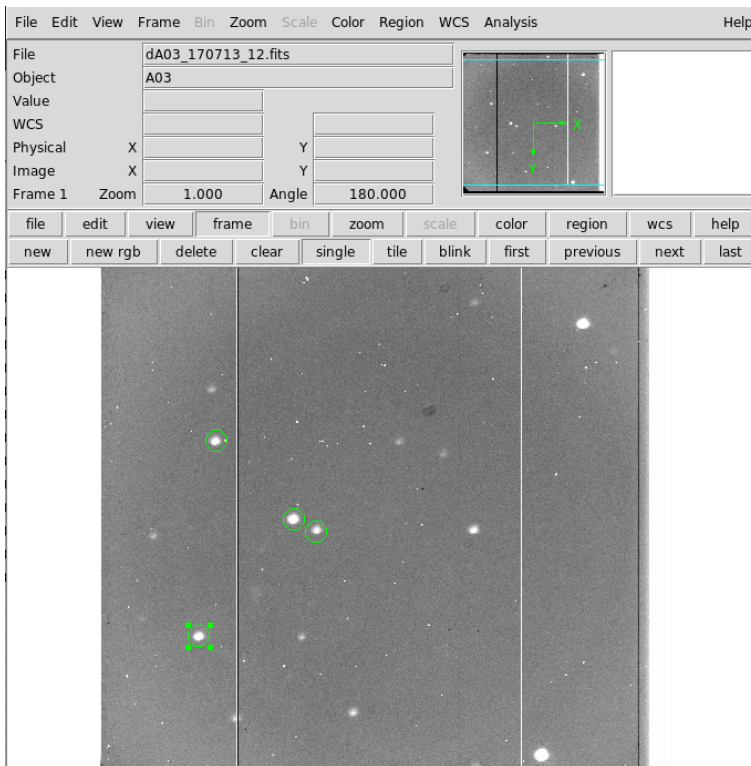
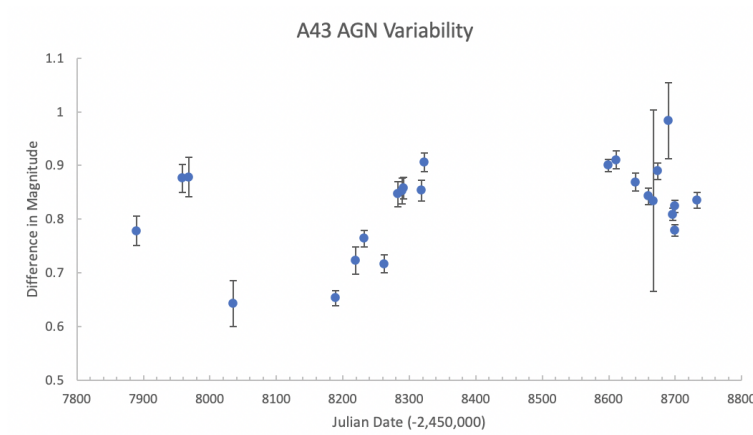Figure 13: Comparison Stars used for object A03.
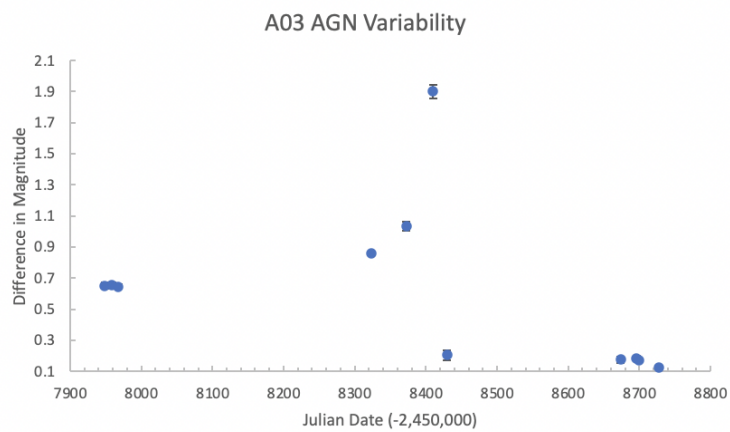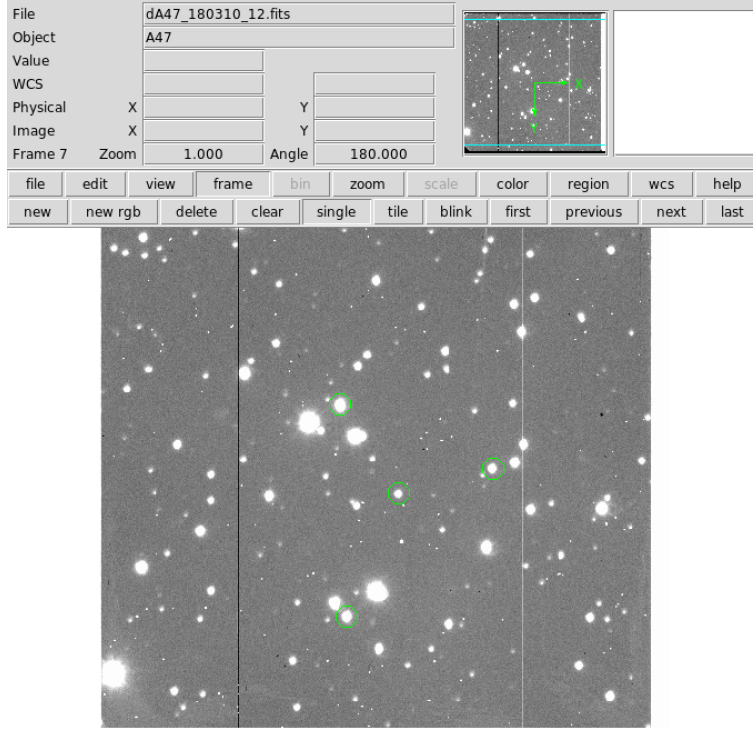

Figure 14: The same as in Figure 5 for object A03.
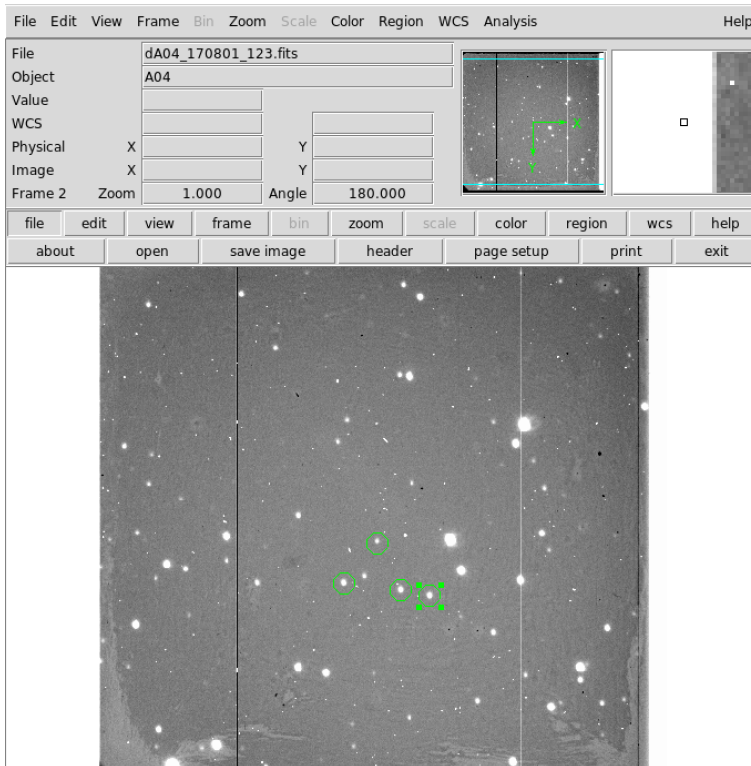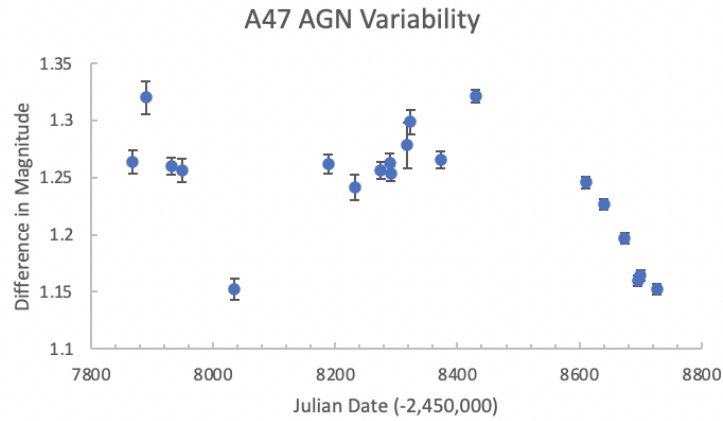
Figure 15: Comparison Stars used for object A04.
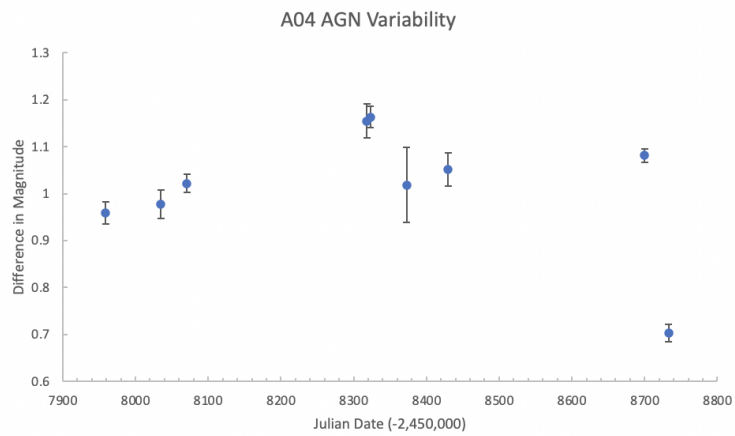
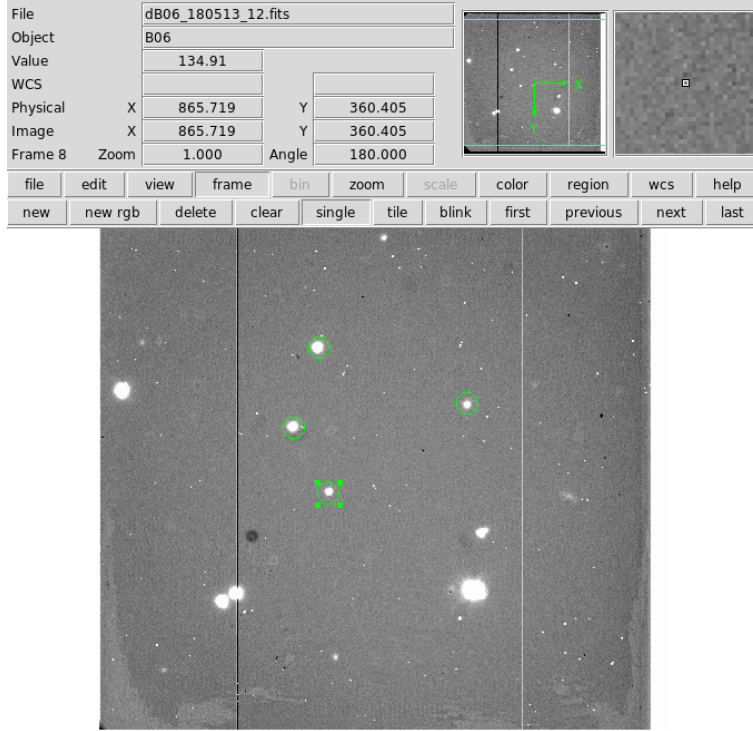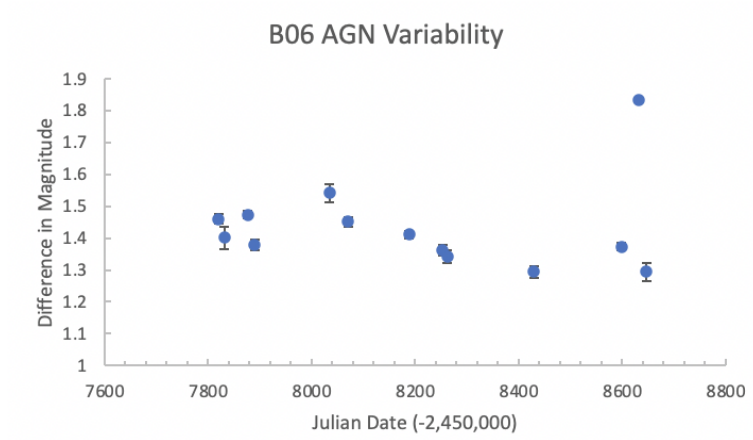Figure 16: The same as in Figure 5 for object A04.
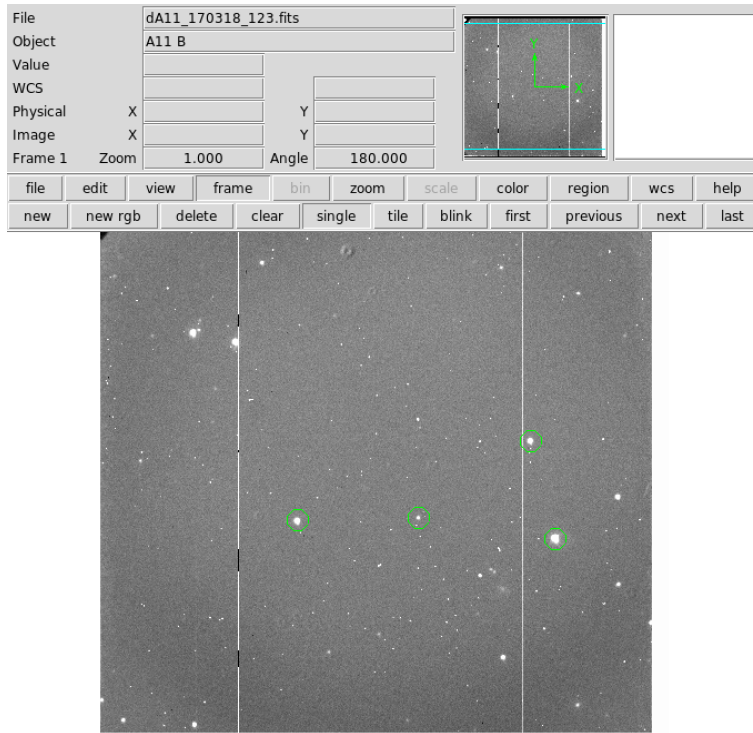
Figure 17: Comparison Stars used for object A11.
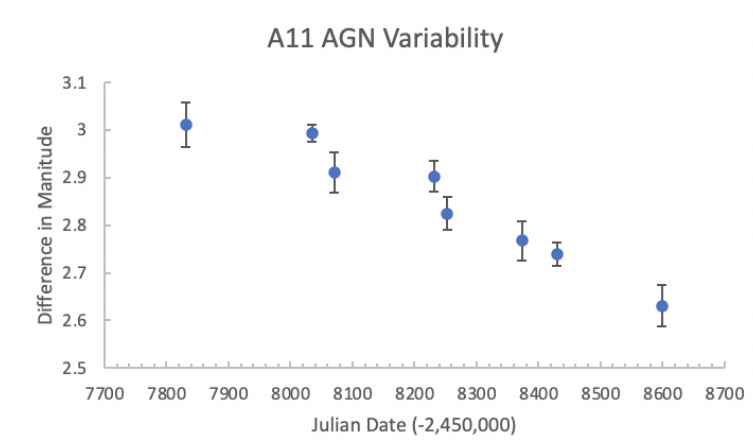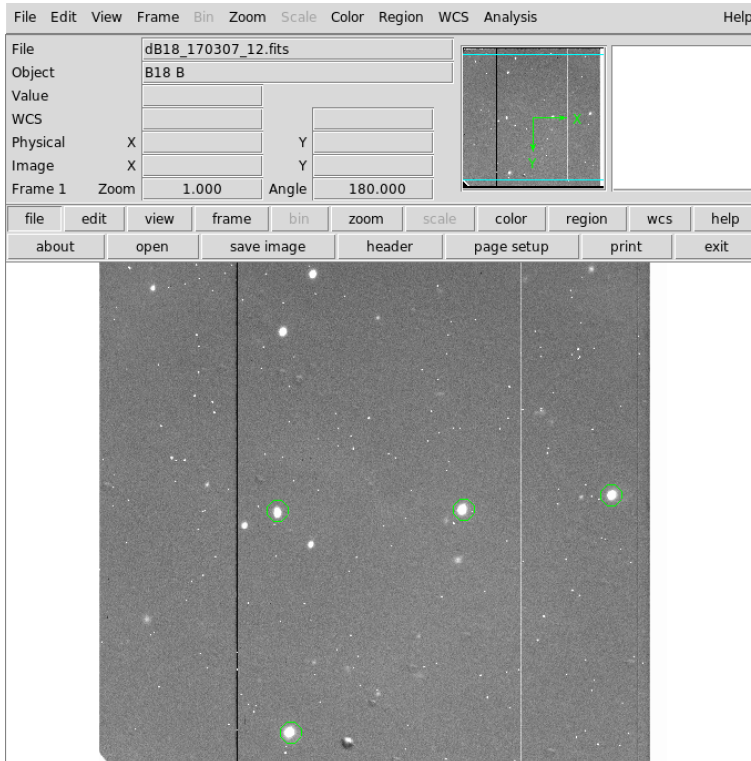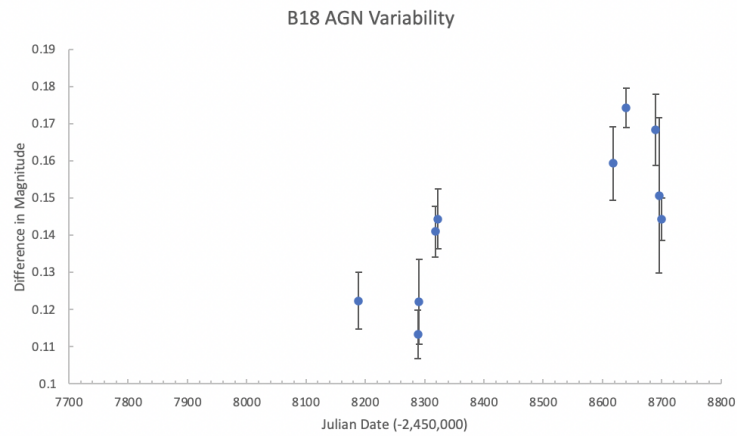

Figure 18: The same as in Figure 5 for object A11.
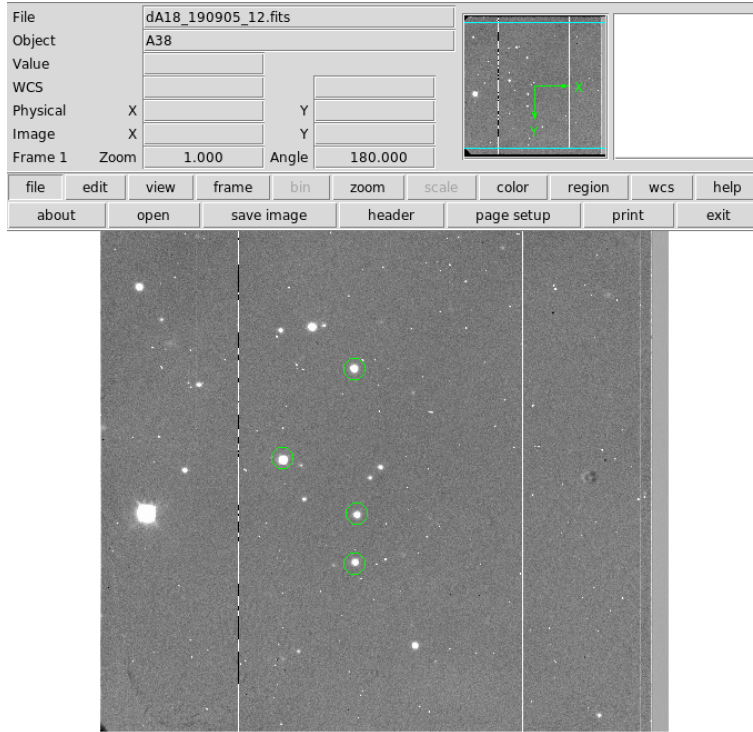
Figure 19: Comparison Stars used for object A18. All images were named A38 instead of A18, but this matches the correct finding chart for A18.
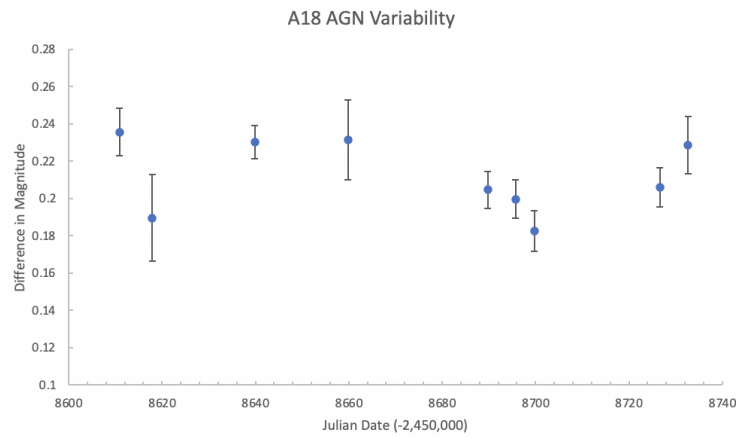
Figure 20: The same as in Figure 5 for object A18.
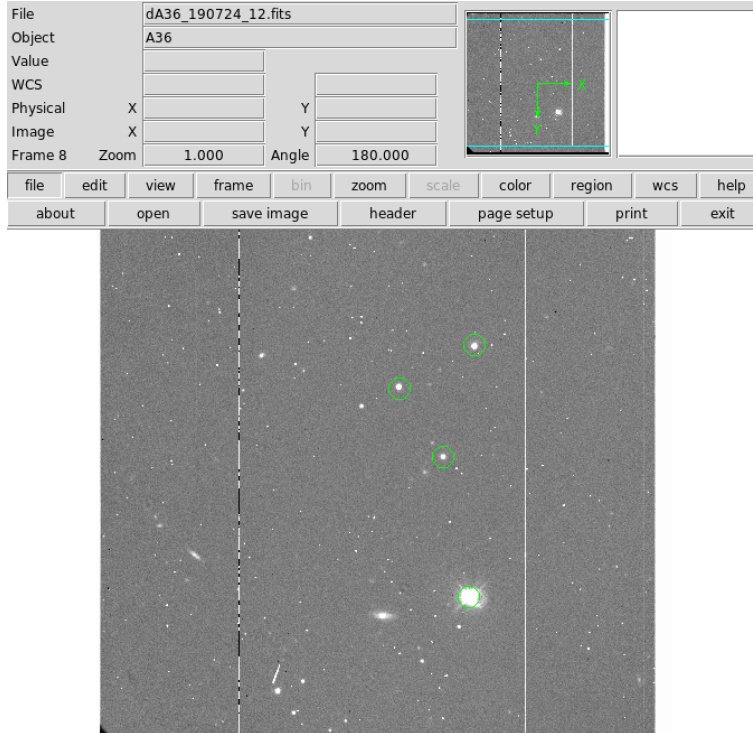
Figure 21: Comparison Stars used for object A36.
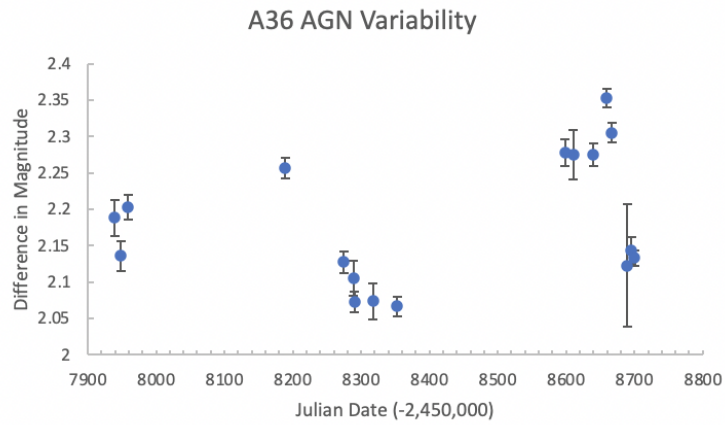
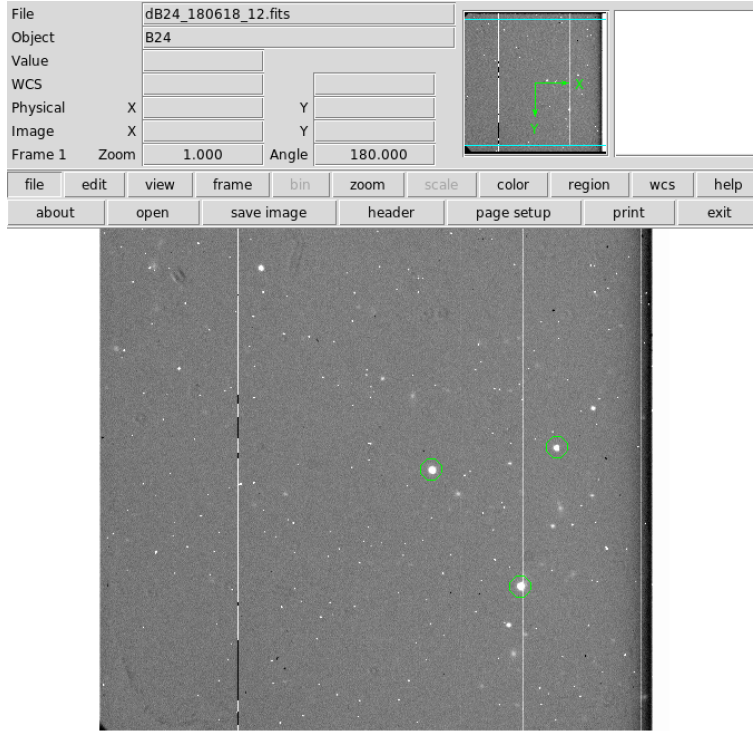

Figure 22: The same as in Figure 5 for object A36.

24
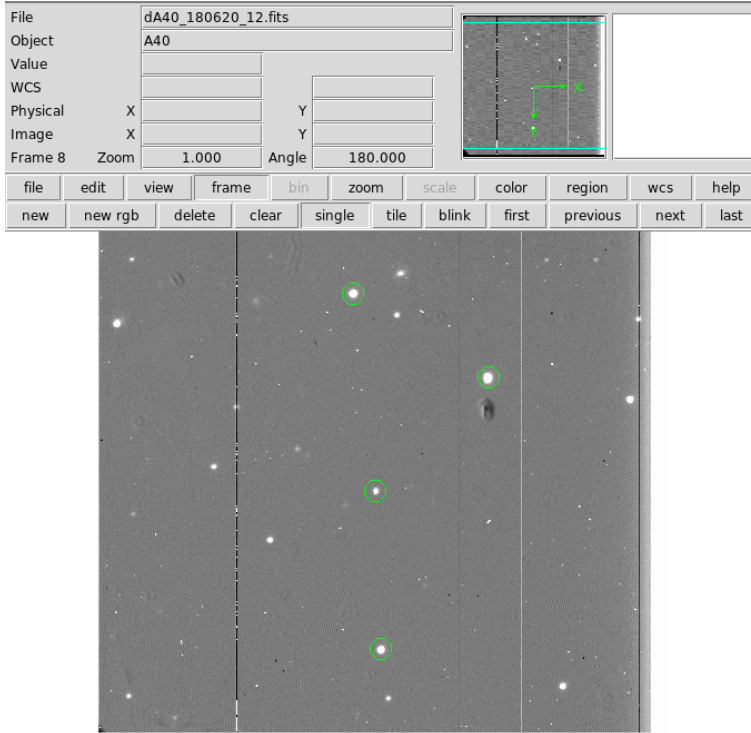
Figure 23: Comparison Stars used for object A40.
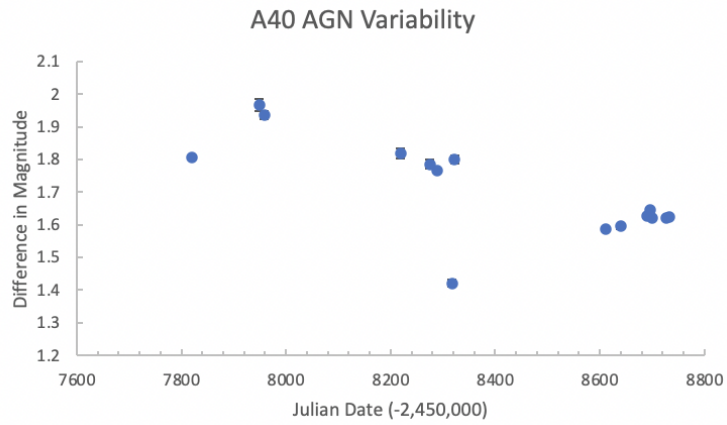
Figure 24: The same as in Figure 5 for object A40.
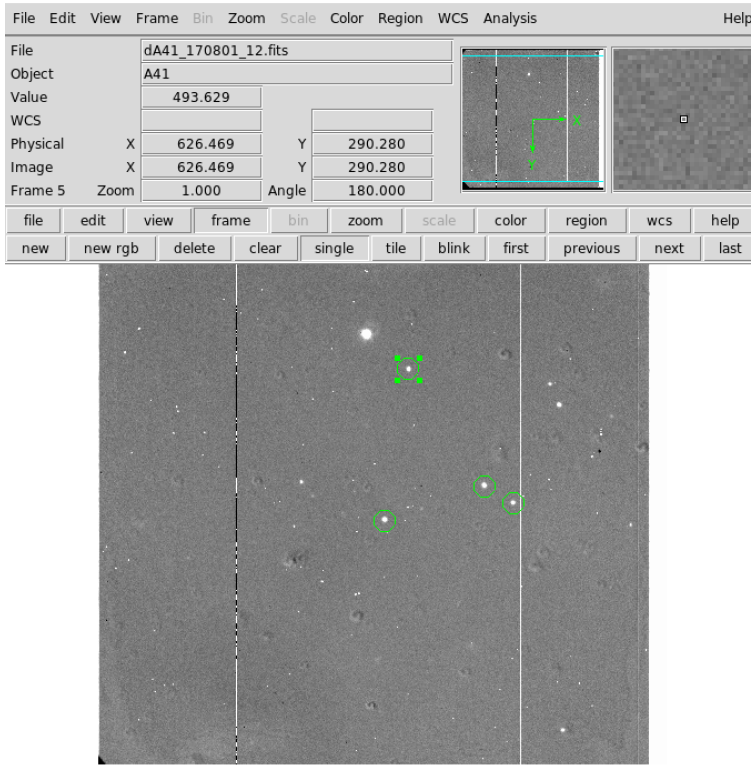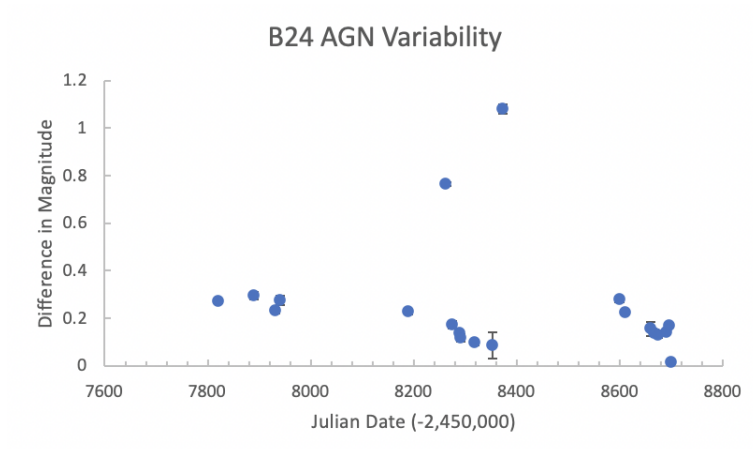
Figure 25: Comparison Stars used for object A41.
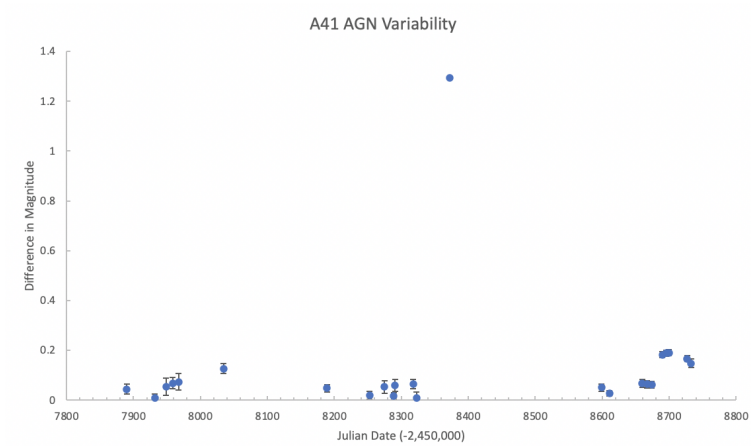
Figure 26: The same as in Figure 5 for object A41.
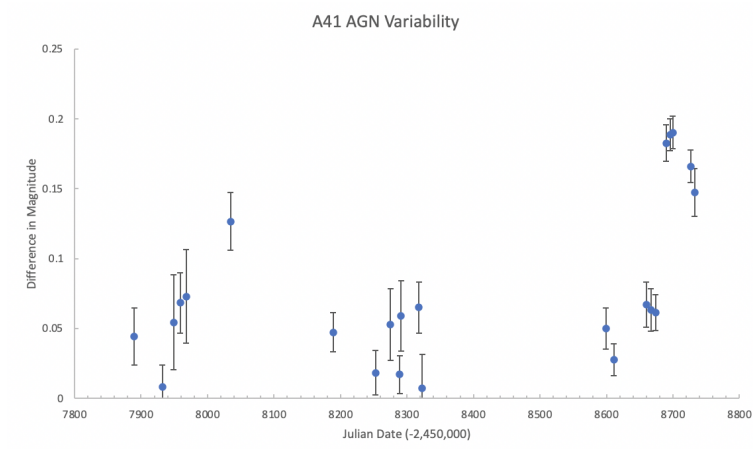
Figure 27: This light curve is the same as the light curve in Figure 24 but without the outlier.
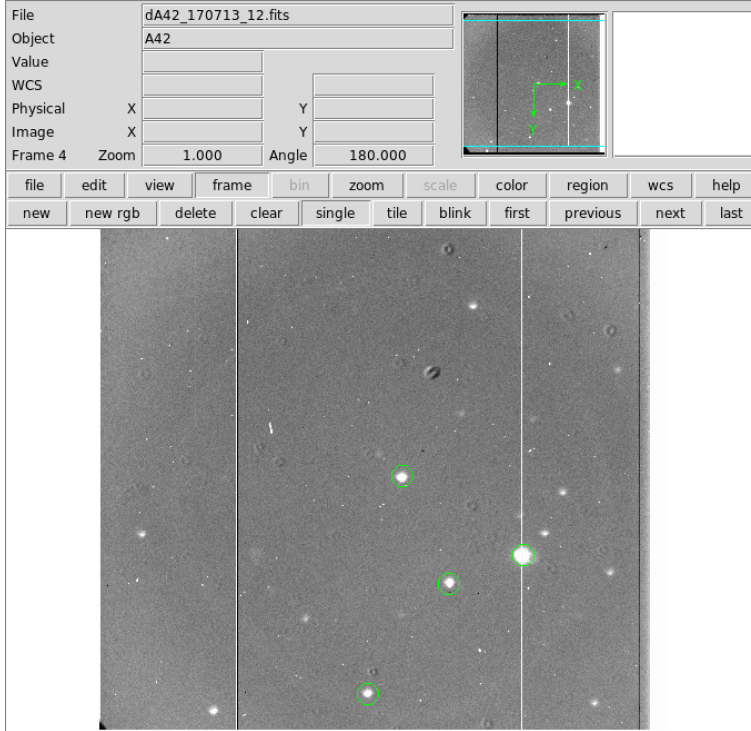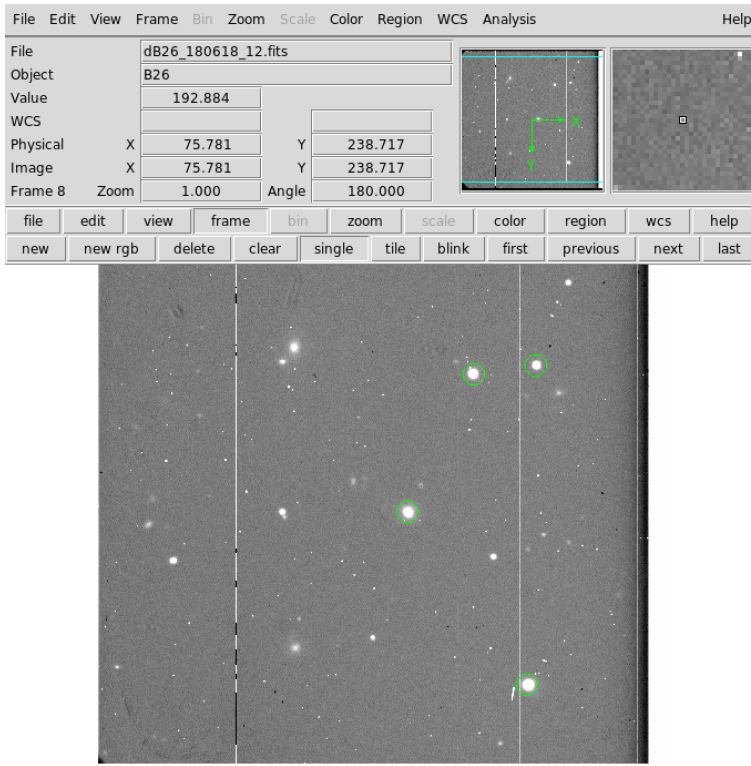
Figure 28: Comparison Stars used for object A42.

Figure 29: The same as in Figure 5 for object A42.
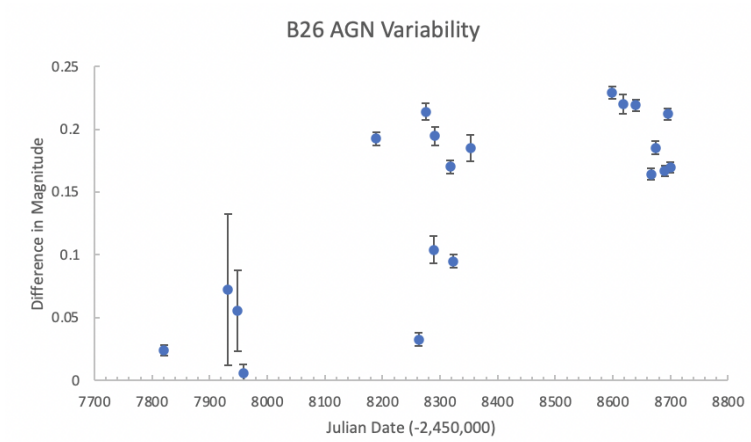
Figure 30: Comparison Stars used for object A43.

Figure 31: The same as in Figure 5 for object A43.

Figure 32: Comparison Stars used for object A47.

Figure 33: The same as in Figure 5 for object A47.

Figure 34: Comparison Stars used for object B06.

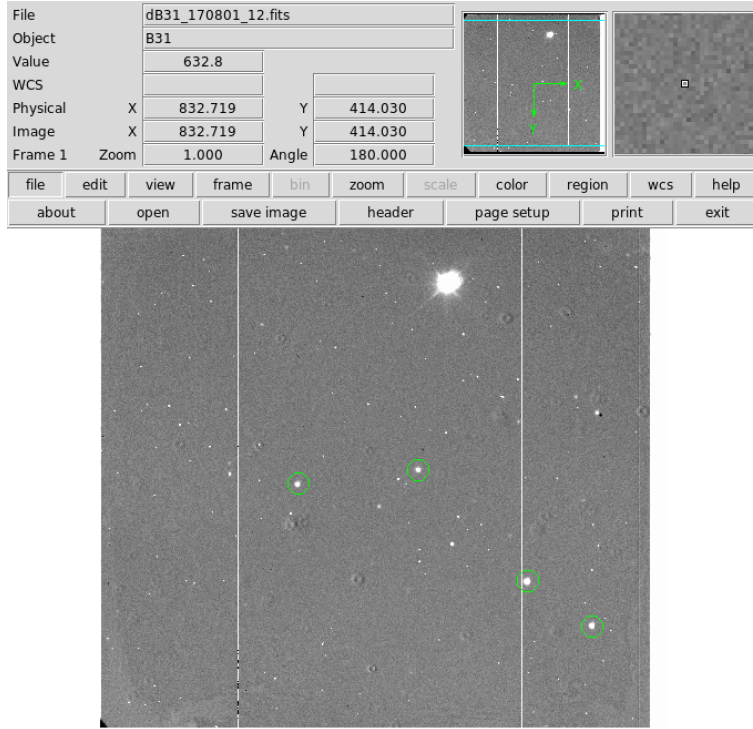Figure 35: The same as in Figure 5 for object B06.

Figure 36: Comparison Stars used for object B18.

Figure 37: The same as in Figure 5 for object B18.

Figure 38: Comparison Stars used for object B24.

Figure 39: The same as in Figure 5 for object B24.

Figure 40: Comparison Stars used for object B26.

Figure 41: The same as in Figure 5 for object B26.
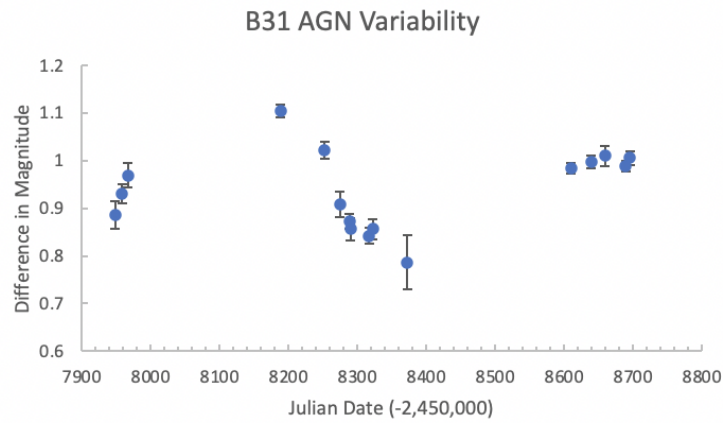
Figure 42: Comparison Stars used for object B31.

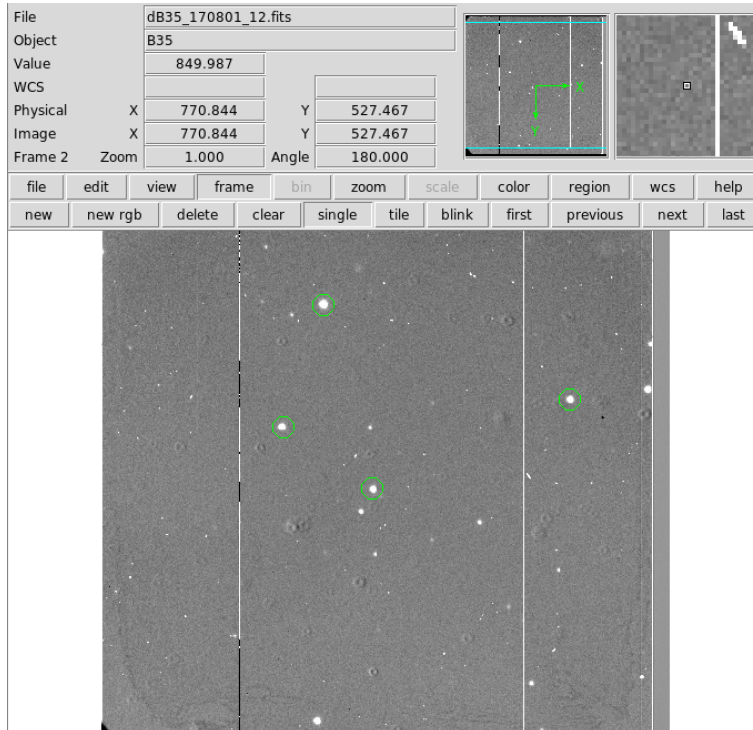Figure 43: The same as in Figure 5 for object B31.
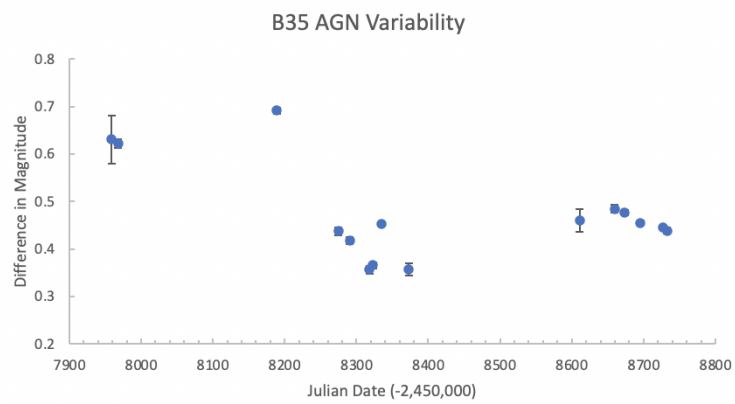
Figure 44: Comparison Stars used for object B35.

Figure 45: The same as in Figure 5 for object B35.